

# Direct detection of self-interacting dark matter

Mark Vogelsberger<sup>1\*</sup> and Jesus Zavala<sup>2,3†</sup>,

<sup>1</sup>*Harvard-Smithsonian Center for Astrophysics, 60 Garden Street, Cambridge, MA 02138, USA*

<sup>2</sup>*Department of Physics and Astronomy, University of Waterloo, Waterloo, Ontario, N2L 3G1, Canada*

<sup>3</sup>*Perimeter Institute for Theoretical Physics, 31 Caroline St. N., Waterloo, ON, N2L 2Y5, Canada*

Accepted ???. Received ???; in original form ???

## ABSTRACT

Self-interacting dark matter offers an interesting alternative to collisionless dark matter because of its ability to preserve the large-scale success of the cold dark matter model, while seemingly solving its challenges on small scales. We present here the first study of the expected dark matter detection signal in a fully cosmological context taking into account different self-scattering models for dark matter. We demonstrate that models with constant and velocity dependent cross sections, which are consistent with observational constraints, lead to distinct signatures in the velocity distribution, because non-thermalised features found in the cold dark matter distribution are thermalised through particle scattering. Depending on the model, self-interaction can lead to a 10% reduction of the recoil rates at high energies, corresponding to a minimum speed that can cause recoil larger than  $300 \text{ km s}^{-1}$ , compared to the cold dark matter case. At lower energies these differences are smaller than 5% for all models. The amplitude of the annual modulation signal can increase by up to 25%, and the day of maximum amplitude can shift by about two weeks with respect to the cold dark matter expectation. Furthermore, the exact day of phase reversal of the modulation signal can also differ by about a week between the different models. In general, models with velocity dependent cross sections peaking at the typical velocities of dwarf galaxies lead only to minor changes in the detection signals, whereas allowed constant cross section models lead to significant changes. We conclude that different self-interacting dark matter scenarios might be distinguished from each other through the details of direct detection signals. Furthermore, detailed constraints on the intrinsic properties of dark matter based on null detections, should take into account the possibility of self-scattering and the resulting effects on the detector signal.

**Key words:** cosmology: dark matter – methods: numerical

## 1 INTRODUCTION

The substantial evidence for the existence of dark matter (DM) accumulated over the last decades, has been purely gravitational in nature. Unambiguous proof of its existence as a new particle beyond the Standard Model (e.g. a supersymmetric particle like the neutralino) relies on a detection through a non-gravitational signature. This is currently one of the most significant challenges for modern astrophysics and particle physics, and it is the reason why many experiments are currently looking for such a signal, either directly trying to measure the recoil of nuclei after a collision with the DM particle, or indirectly by measuring the byproducts of its self-annihilation (see Bertone et al. 2005, for a review).

The interaction rate of DM particles with experiment targets at laboratories on Earth not only depends on the mass and interaction cross section of DM but also on its local phase-space distribution

at the scale of the apparatus. Any hope of extracting information about the nature of DM relies therefore on detailed knowledge of the latter. Numerical simulations that follow the gravitational collapse of the primordial DM density perturbations have been very successful in reproducing the large-scale structure of the Universe (e.g. Springel et al. 2005) and provide detailed predictions on the internal structure of DM haloes (e.g. Springel et al. 2008; Diemand et al. 2008; Stadel et al. 2009; Wu et al. 2012). These simulations are the most reliable approach to study structure formation (see Kuhlen et al. 2012, for a recent review) and its importance for direct detection experiments has been pointed out recently, by finding departures from the traditional assumptions: a smooth density distribution and a Maxwellian velocity distribution. It was found that the phase-space distribution of relaxed DM haloes is not featureless but contains imprints of its formation history in the energy distribution (e.g. Vogelsberger et al. 2009; Kuhlen et al. 2010, 2012). Over the last years it also became possible to study the fine-grained phase-space structure of DM by extending classical N-body methods (Vogelsberger et al. 2008; White & Vogelsberger 2009; Vogels-

\* Hubble Fellow, mvogelsb@cfa.harvard.edu

† CITA National Fellow

berger et al. 2009; Vogelsberger & White 2011; Abel et al. 2011; Neyrinck & Shandarin 2012).

An important point to be made about these simulations is that most of them, certainly the ones used for estimating direct detection rates, assumed a Cold DM (CDM) cosmology. In this model, DM particles are thought to be cold (i.e., the thermal motions of DM particles were essentially negligible at the time of matter-radiation equality) and collisionless (i.e., negligible self-interaction). The possibility remains, however, that one or both of these hypothesis are not true on all scales. In fact, the evidence that supports them clearly allows for significant DM self-scattering (e.g. Peter et al. 2012) and for the possibility of DM being warm (e.g. Boyarsky et al. 2009). Indeed, the alternative self-interacting DM (SIDM) and Warm DM (WDM) models are attractive possibilities to solve some of the current challenges to CDM at the scale of dwarf galaxies without spoiling its successes at larger scales (e.g. Colín et al. 2000; Bode et al. 2001; Zavala et al. 2009; Spergel & Steinhardt 2000; Loeb & Weiner 2011; Vogelsberger et al. 2012; Rocha et al. 2012). The SIDM possibility is particularly exciting since it is not in conflict with current astrophysical constraints, such as the shape of DM haloes and the survivability of satellite haloes (Loeb & Weiner 2011; Peter et al. 2012), and is able to produce central density cores that are seemingly consistent with observations of dwarf galaxies at different scales (see Rocha et al. (2012) and Vogelsberger et al. (2012), hereafter VZL). The scattering cross section is assumed to be either constant or velocity dependent. In the constant cross section case, tight constraints have been derived using halo shapes based on X-ray and lensing data from ellipticals and galaxy clusters: the momentum-transfer weighted cross section  $\sigma_T/m_\chi$  is likely  $< 1 \text{ cm}^2 \text{ g}^{-1}$  by current estimates (e.g. Peter et al. 2012). Until very recently, it was not clear if it was possible to solve all outstanding small-scale CDM problems in a constant cross section scenario with a value lower than currently allowed. For example, Yoshida et al. (2000) argued that for  $\sigma_T/m_\chi \sim 0.1 \text{ cm}^2 \text{ g}^{-1}$ , the collision rate would be too low to create sizable cores in dwarf galaxies while Rocha et al. (2012) suggests that values in this ballpark would be sufficient, but both of these contradictory claims are based on simulations that do not resolve the scales in dispute. In Zavala et al. (2012) we used the simulations presented in this paper to clarify this issue showing that a constant scattering cross section is a viable explanation for the low dark matter densities inferred in the Milky Way (MW) dwarf spheroidals only within the very narrow range:  $0.6 \text{ cm}^2 \text{ g}^{-1} \leq \sigma_T/m_\chi \leq 1.0 \text{ cm}^2 \text{ g}^{-1}$ . On the other hand, a model with a velocity dependent cross section can easily circumvent cluster constraints, but preserve the SIDM effects on small scales by adopting an appropriate velocity dependence.

The magnitude of the self-interacting cross section for GeV-scale DM particles needed to produce a significant impact at the scale of dwarf galaxies is of the order of the strong interaction cross section for neutron-neutron or neutron-proton scattering. This does not at all imply that DM should interact with nuclei through the strong nuclear force. If that were the case, DM particles would not reach ground-based detectors that are looking for Weakly Interacting Massive Particles (WIMPs), since they would scatter in the atmosphere and reach the ground with energies below the threshold of current experiments. Also, any kind of shielding would further prevent detection of strongly interacting DM. Significant constraints on this type of DM are therefore obtained with space-based instruments (Erickcek et al. 2007). Instead, an example of the particle physics model we imagine here is that presented in Hooper et al. (2012). In this type of hidden-sector DM, a new gauge boson that has a small kinetic mixing with the photon can result in elastic scat-

Name	$\sigma_T^{\text{max}}/m_\chi [\text{cm}^2 \text{ g}^{-1}]$	$v_{\text{max}} [\text{km s}^{-1}]$
CDM	/	/
SIDM10	10	/
SIDM1	1	/
SIDM0.1	0.1	/
vdSIDMa	3.5	30
vdSIDMb	35	10

**Table 1.** DM models considered in this paper. CDM is the standard collisionless model without any self-interaction. SIDM10 is a reference model with a constant cross section much larger than allowed by current observational constraints. vdSIDMa and vdSIDMb have a velocity-dependent cross section motivated by the particle physics model presented in Loeb & Weiner (2011), are allowed by all astrophysical constraints, and solve the “too big to fail” problem (see Boylan-Kolchin et al. 2011) as demonstrated in VZL. SIDM1 and SIDM0.1 were not discussed in VZL, and are constant cross section scenarios with 10/100 times smaller transfer cross section than SIDM10. They were considered recently by Rocha et al. (2012) and Peter et al. (2012).

tering of DM with protons at the level of what is hypothetically seen by the DAMA experiment (Bernabei et al. 2012). The same gauge boson can act between the DM particles to enhance self-scattering (e.g. Buckley & Fox 2010; Loeb & Weiner 2011; van den Aarssen et al. 2012). Another example of a similar model is given by Forngeno et al. (2011), while another distinct possibility is that of the Atomic Dark Matter model (see Cyr-Racine & Sigurdson 2012).

If DM is indeed self-interacting, then direct detection experiments should assume the appropriate DM phase-space distribution and not the one based on CDM simulations. The purpose of this paper is to study the SIDM local density and velocity distribution using high resolution cosmological simulations and to quantify the difference between currently allowed SIDM models and CDM. In particular, we estimate the impact of self-scattering on the expected interaction rates with nuclei and its signature in direct detection experiments.

The paper is organised as follows. In Section 2 we present the SIDM models we consider and details of our simulation suite. Section 3 presents general results on the coarse-grained phase-space structure in the inner halo. In Section 4 we focus on the velocity structure of the different models and contrast them to the CDM case. Here we also show that our results are valid for generic MW like haloes, i.e. they are not sensitive to cosmic variance. The differences in the velocity distribution directly impact the direct detection signal as we demonstrate in Section 5. Finally, we give our conclusions in Section 6.

## 2 SIDM MODELS AND SIMULATIONS

In VZL we followed the formation and evolution of a single MW-size halo (simulated at different resolutions) in the context of a few benchmark points within elastic velocity-dependent SIDM models. In these models, linear momentum and energy are conserved during a scatter event, but the direction of the relative velocity vector is randomly redistributed resulting in isotropic scattering. We refer the reader to VZL for details and testing of our Monte Carlo based self-scattering algorithm, and its implementation within the

Name	$m_p [M_\odot]$	$\epsilon [\text{pc}]$	$M_{200} [M_\odot]$	$r_{200} [\text{kpc}]$
Aq-A-3	$4.911 \times 10^4$	120.5	$1.836 \times 10^{12}$	245.64
Aq-A-4	$3.929 \times 10^5$	342.5	$1.838 \times 10^{12}$	245.70
Aq-B-4	$2.242 \times 10^5$	342.5	$8.345 \times 10^{11}$	188.85
Aq-C-4	$3.213 \times 10^5$	342.5	$1.793 \times 10^{12}$	243.68
Aq-D-4	$2.677 \times 10^5$	342.5	$1.791 \times 10^{12}$	243.60
Aq-E-4	$2.604 \times 10^5$	342.5	$1.208 \times 10^{12}$	213.63
Aq-F-4	$1.831 \times 10^5$	342.5	$1.100 \times 10^{12}$	206.60

**Table 2.** Parameters of the Aquarius simulations.  $m_p$  is the DM particle mass,  $\epsilon$  is the Plummer equivalent gravitational softening length.  $M_{200}$  is the virial mass of the halo, defined as the mass enclosed in a sphere with mean density 200 times the critical value and  $r_{200}$  gives the corresponding virial radius (both for the CDM case). We mainly focus on Aq-A-3 and study how the different DM models affect its phase-space structure. The level-4 haloes are only used to estimate how cosmic variance affects the results.

GADGET-3 code for cosmological simulations (last described in Springel (2005)). For this paper, we extend the simulation suite presented in VZL by adding two more SIDM benchmark models with a constant cross section (see Table 1) and more individual haloes to study the effect of cosmic variance allowing us to have a range of MW-size haloes with different formation histories, subhalo abundance, environments, etc. The initial conditions for our simulations are taken from the Aquarius Project (Springel et al. 2008) with the following cosmological parameters:  $\Omega_m = 0.25$ ,  $\Omega_\Lambda = 0.75$ ,  $h = 0.73$ ,  $\sigma_8 = 0.9$  and  $n_s = 1$ ; where  $\Omega_m$  and  $\Omega_\Lambda$  are the contribution from matter and cosmological constant to the mass/energy density of the Universe, respectively,  $h$  is the dimensionless Hubble constant parameter at redshift zero,  $n_s$  is the spectral index of the primordial power spectrum, and  $\sigma_8$  is the rms amplitude of linear mass fluctuations in  $8 h^{-1}$  Mpc spheres at redshift zero.

In Table 1 we list the different SIDM models we consider in this paper. CDM is the vanilla collisionless case and SIDM10 only serves as a test case to demonstrate the effects of a large constant cross section (already ruled out by various astrophysical constraints). vdSIDMa and vdSIDMb on the other hand are velocity-dependent SIDM (vdSIDM) cases, that do not violate any astrophysical constraints and are well-motivated from a particle physics point of view (e.g. Arkani-Hamed et al. 2009; Loeb & Weiner 2011). They produce  $\mathcal{O}(1 \text{ kpc})$  density cores in the MW subhaloes as discussed in VZL. We extended our sample here by adding SIDM1 which has a constant cross section ten times smaller than SIDM10, bringing it closer to current constraints although it is still above them as recently pointed out by Peter et al. (2012). SIDM0.1 has an even smaller constant cross section of  $\sigma_T/m_\chi = 0.1 \text{ cm}^2 \text{ g}^{-1}$ , which is consistent with all astrophysical observations including cluster scale constraints (for further details, see Peter et al. 2012). In Fig. 1 we show the transfer cross sections as a function of relative velocity for all the benchmark models. The cross section of the vdSIDM models falls off as  $v^{-4}$  towards larger relative velocities. They can therefore have a quite large cross section at smaller velocities without violating cluster constraints. For example, at  $v = 10 \text{ km s}^{-1}$  the vdSIDM models have cross sections even larger than SIDM10.

In VZL we simulated the elastic models CDM, SIDM10, vd-

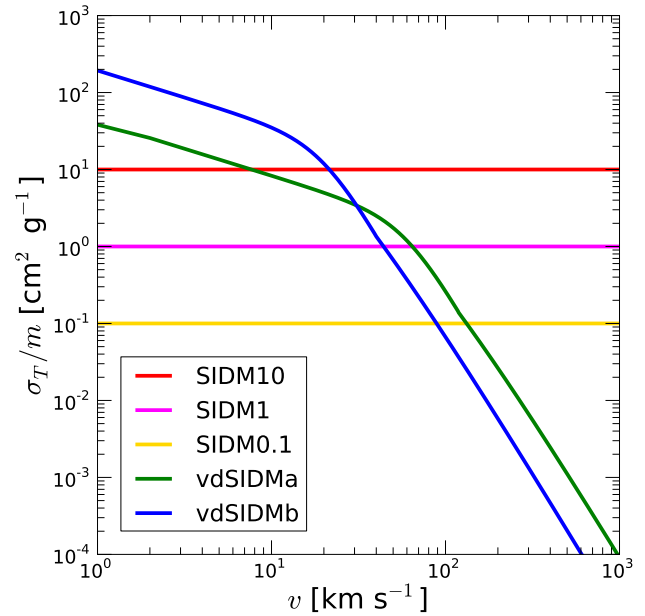


**Figure 1.** Dependence of the transfer cross section on the relative velocity for the different SIDM models (see Table 1). SIDM10, SIDM1, SIDM0.1 are models with constant cross sections differing by factors of ten ranging from  $\sigma_T/m_\chi = 0.1 \text{ cm}^2 \text{ g}^{-1}$  (SIDM0.1) to  $\sigma_T/m_\chi = 10 \text{ cm}^2 \text{ g}^{-1}$  (SIDM10). The vdSIDMa and vdSIDMb models have a velocity-dependent cross section with slightly different peak values and velocities where the cross section is maximal. vdSIDMa, vdSIDMb and SIDM0.1 are compatible with astrophysical constraints. SIDM1 is likely too large to be consistent with cluster observations, whereas SIDM10 is clearly ruled out and mainly serves here as a test scenario to demonstrate the various effects. The vdSIDM models fall off as  $v^{-4}$  for higher relative velocities which allows for large cross sections towards lower velocities. Cluster constraints can then be easily circumvented for such models, whereas they impose a clear upper limit for the constant cross section models.

SIDMa and vdSIDMb for the Aq-A halo at resolution levels 3, 4 and 5, corresponding to an approximate spatial resolution (given by  $2.8\epsilon$ , where  $\epsilon$  is the Plummer equivalent gravitational softening length) of about 2.0 kpc, 1.0 kpc, and 0.3 kpc, respectively. The exact mass resolution depends on the particular halo, but is of the order of  $10^6 M_\odot$ ,  $10^5 M_\odot$ , and  $10^4 M_\odot$  for level 5, 4, and 3, respectively. The simulation details are summarised in Table 2, where we also specify the virial properties of the different haloes.

We extend the original simulation suite and simulate the remaining SIDM models (SIDM1, SIDM0.1) at resolution level 3. We also explore here five other Aquarius haloes (labelled Aq-B to Aq-F) at level 4 resolution for all the SIDM cases. The full set of Aquarius haloes covers a wide range of formation histories and virial masses of MW-type haloes, allowing us to bracket the uncertainties in the local phase-space distribution due to halo-to-halo scatter, see Springel et al. (2008) for details. Resolution level 4 is sufficient to accomplish this.

### 3 PHASE SPACE STRUCTURE

We examine here first the inner coarse-grained phase-space distributions of the Aquarius Aq-A-3 halo for the different SIDM models, and contrast them to the CDM case. In Fig. 2, we show the phase-space structure weighting the simulation particles by their local coarse-grained phase-space density  $\rho/\sigma^3$ , where  $\rho$  and  $\sigma$  are

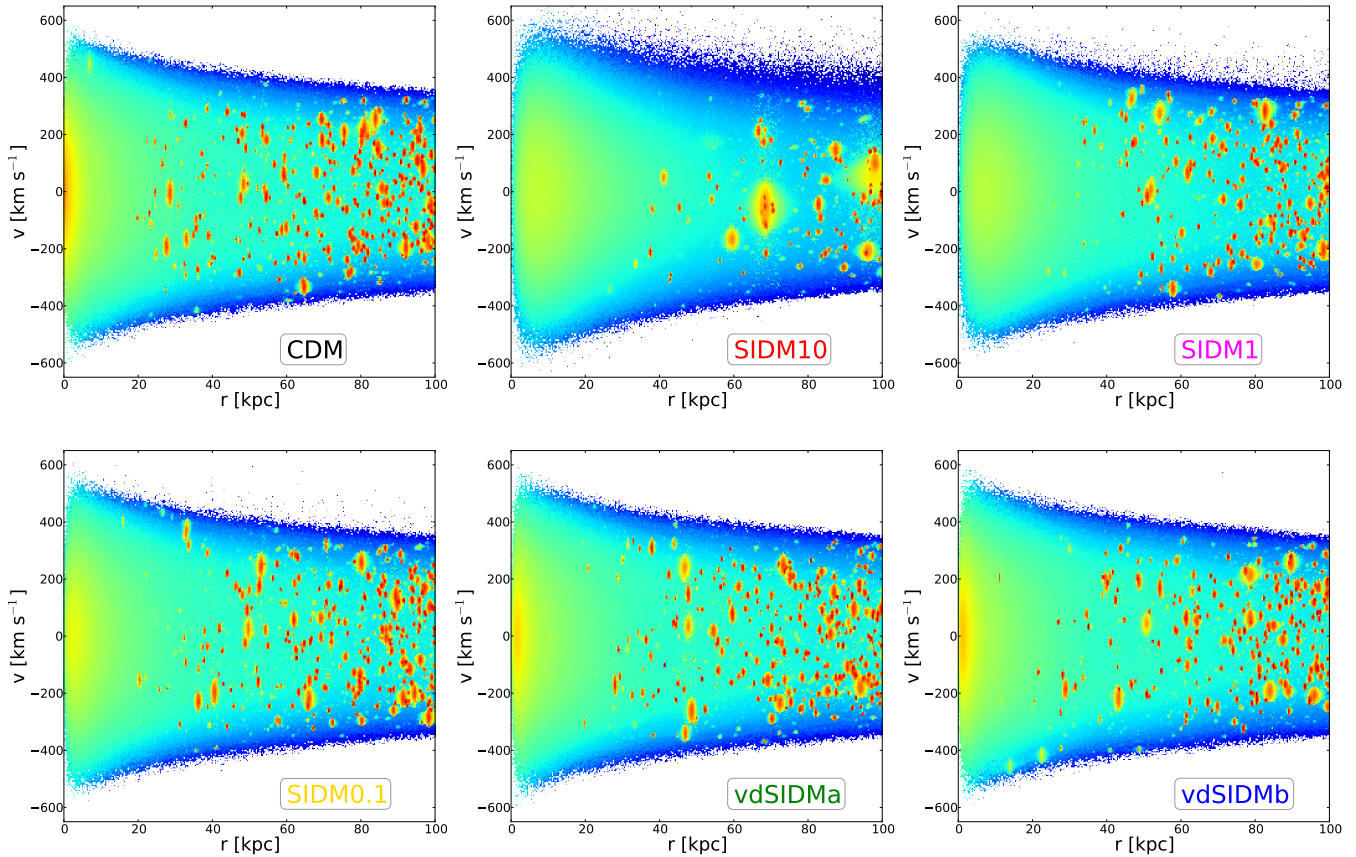


**Figure 2.** Phase-space histograms of all DM models considered in this work. The contribution of each particle is weighted by its local coarse-grained phase-space density  $\rho/\sigma^3$ . SIDM10 leads to a significant suppression of substructure, and also to a strong reduction of the central main halo phase-space density. Although SIDM1 has a ten times smaller constant cross section it still shows a strong reduction of the central main halo phase-space density, but the abundance of substructure is similar to the CDM case. The former effect is nearly absent for vdSIDMa and vdSIDMb because the cross section is velocity-dependent in these cases, which compensates for the rising configuration space density towards the center. In these cases, it is also apparent that the phase-space density in substructures is lower than in CDM. SIDM0.1, with the smallest constant cross section, still looks different from the vdSIDM models in the center of the main halo even though the substructure distribution looks very similar.

calculated based on SPH estimates using 64 neighbours. Except for SIDM10, where (sub)haloes are significantly more spherical and less dense (as demonstrated in VZL), the phase-space structure of the different models looks rather similar to the CDM case, albeit all of them produce density cores. The core density of the main halo is lower for the constant cross section models than for the vdSIDM models. Although SIDM1 (SIDM0.1) has a constant cross section that is ten (a hundred) times smaller than in SIDM10, there is still a noticeable reduction of the central phase-space density of the main halo. This effect is nearly absent for the vdSIDMa and vdSIDMb models due to the velocity-dependence of their cross sections, which compensates for the rising configuration space density towards the center. This then leads to a reduced scatter rate in the center and therefore the central phase-space density is not significantly reduced for the models with velocity-dependent cross section. We note that except for SIDM10, all models have a subhalo abundance that is very similar to the one in CDM.

For the self-interacting models we can also weight the bins in the phase-space distribution by the number of scattering events (until  $z = 0$ ), as we show in the leftmost column of Fig. 3. Specifically, we are plotting the mean mass-weighted number of scatter events for each phase-space bin. We note that we do not use the same

colour scales for the different models in order to show the details in each case more clearly. The actual numbers of scatter events are indicated by the colour bars. As expected, the centres of the main halo and its subhaloes have the highest numbers of scatter events, although in the constant cross section cases (particularly in SIDM10) individual subhaloes are not easily distinguishable in this phase-space projection with most of the particles having encountered a large number of scatter events until  $z = 0$ . vdSIDMa and vdSIDMb look very similar to each other and significantly different from all constant cross section models. The central main halo region, with large scatter counts, is more extended in the latter whereas it is very small for the vdSIDM models since the velocity scaling of the cross section compensates the increasing density towards the main halo center leading to a suppression of scattering events. Subhaloes are clearly visible in the vdSIDM models since self-scattering is enhanced in these cold (low velocity) and dense structures. We note that this behaviour depends on the details of the vdSIDM models. Specifically, it depends on the velocity at which the cross section peaks. As shown in Fig. 1, vdSIDMa and vdSIDMb both peak at rather low velocities, which was chosen specifically to get significant self-scatterings at the scale of dSphs (see VZL). Other choices of the peak velocity will lead to different phase-space structures.

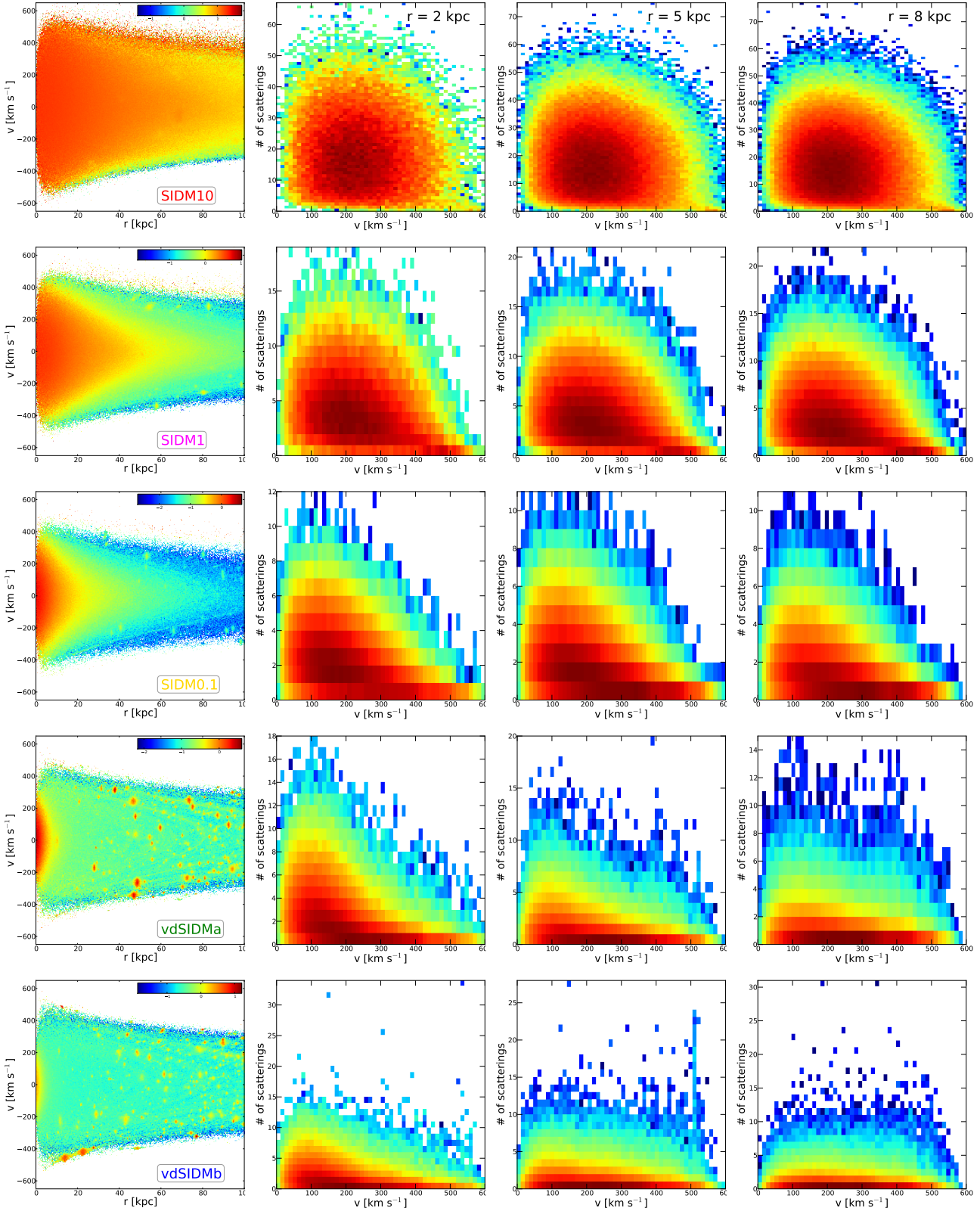


**Figure 3.** Left column: Phase-space histograms where each pixel represents the mean mass-weighted number of scatterings that particles in that bin underwent until  $z = 0$  (see colorbar). Remaining columns: Number of particle scatterings ( $y$ -axis) as a function of velocity modulus ( $x$ -axis). Colours indicate the mass in each bin. We show the distributions for three different distances (second column: 2 kpc; third column: 5 kpc; fourth column: 8 kpc) and in all cases for 1000 observers. The distribution is measured within spheres of 1 kpc radius. The number of particles with large number of scatterings increases strongly towards the main halo center for all models. The constant cross section cases look similar, although SIDM10 shows clearly a very large number of scattering events until  $z = 0$ . On the other hand, the vdSIDM models have a steeper distribution of the scattering events towards the center of the (sub)haloes, where DM is colder and denser. Notice how subhaloes are clearly highlighted in the left column for these cases.

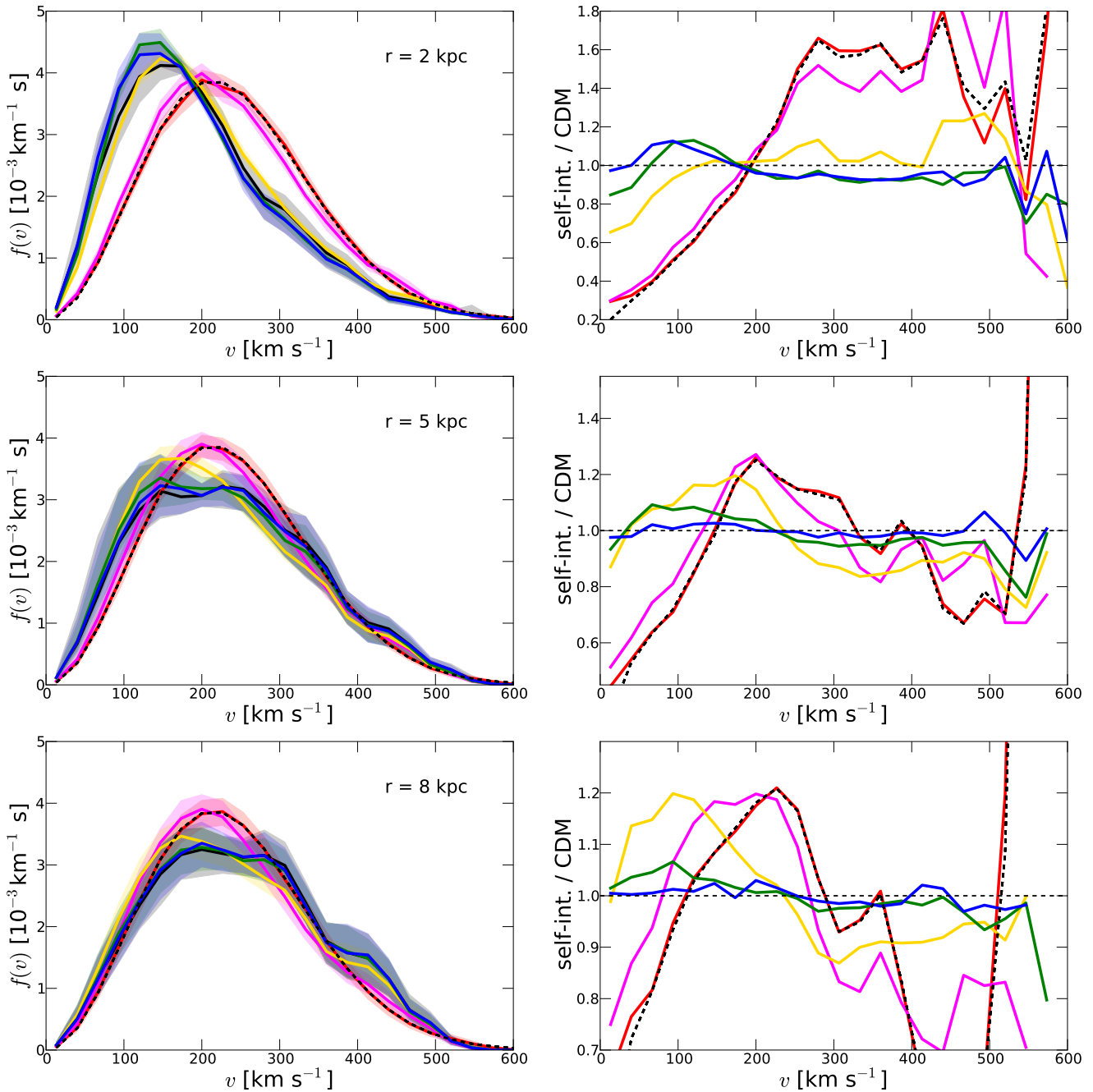


**Figure 4.** Left panels: Distribution of the velocity modulus measured in spheres of 1 kpc radius for 1000 random positions at a given halocentric distance (as indicated). The median and 10 – 90% quantiles of the distribution (over all observers) are shown with solid thick lines and shaded regions, respectively. Right panels: The median of the ratio of the velocity distributions to the CDM case for each observer. Colours are as in Fig. 1. The mean free path of the DM particles is shortest in the halo center, creating the largest differences between the self-interacting and CDM models. For larger radii, the decrease in the density diminishes the scattering rate and hence the local velocity distributions are more similar. The large and constant cross section of SIDM results in a smooth and isotropic Maxwellian distribution at all radii within the core region ( $\sim 10 \text{ kpc}$ ). To lower extent, SIDM1 and SIDM0.1 with 10 and 100 times lower constant cross section, respectively, still show clear deviations from CDM. On the contrary, at 8 kpc, the velocity-dependent SIDM cases (vdSIDMa and vdSIDMb) deviate from the CDM model by at most 5%. The dashed black line in the left panels shows a Maxwell-Boltzmann distribution with  $\sigma_{1D} = 151.6 \text{ km s}^{-1}$ , which fits the SIDM10 distribution very well. The distribution of SIDM1 is still quite Maxwellian, whereas all other models clearly have very different distributions

To study the relation between scattering events and the local velocity structure in more detail we also show in Fig. 3 histograms of the local velocity modulus versus the number of scatterings (until  $z = 0$ ) at three halocentric distances: 2 kpc (second column), 5 kpc (third column) and 8 kpc (fourth column). The largest con-

stant cross section case SIDM10 shows a very large number of scattering events within a 10 kpc region from the center. In this region, most of the particles have been scattered multiple times creating a constant isothermal density core (see VZL). This process of transforming the velocity distribution into a Maxwellian one is incom-

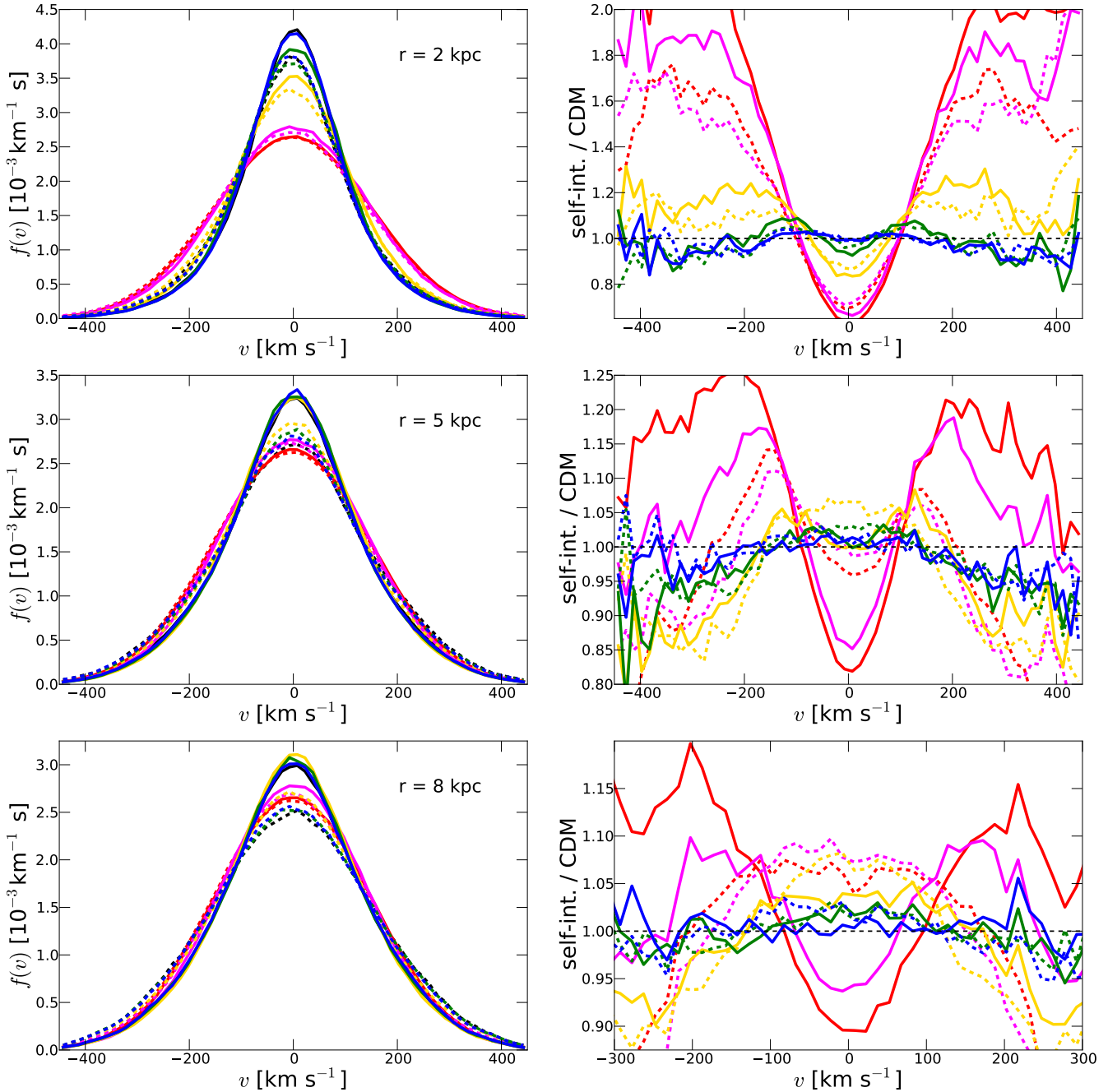


**Figure 5.** Left panels: Velocity distribution along the largest (solid) and smallest (dashed) components of the local velocity ellipsoid measured in spheres of 1 kpc radius for 1000 random positions at a given halocentric distance (as indicated). Only the median of the distributions is shown. Right panels: Median of ratio of each distribution to the corresponding CDM case. Colours are as in Fig. 1. Compared to the SIDM models CDM haloes are more anisotropic in the inner regions (see also Fig. 6), whereas the SIDM models clearly show a velocity ellipsoid which is much more spherical, particularly for the cases with a large constant cross section. At the solar circle, the relative deviations between the models and CDM is rather small, particularly for the vdSIDM models, although the SIDM10 and SIDM1 cases still show some significant differences.

plete for the SIDM1 and SIDM0.1 cases where the cross section is much lower. On the other hand, for the vdSIDM cases most of the scatter events have occurred within 1 kpc which is the region with the lowest velocity dispersion and highest density.

We note that in our analysis we are not including the effects of baryonic physics on the DM phase-space structure. Typically, predictions on direct detection signals are obtained without considering these effects. It is expected that the domination of the cen-

tral gravitational potential by the galactic disc might alter dramatically the inner DM distribution, flattening the central cusp in CDM haloes due to repeated episodes of gas outflows driven by supernovae (e.g. Navarro et al. 1996; Pontzen & Governato 2012). Another process that might impact the inner DM phase-space structure are resonant interactions between the DM particles and the stellar bar (e.g. Weinberg & Katz 2002). DM subhaloes are also affected if they tidally interact with the galactic disc (e.g. D’Onghia

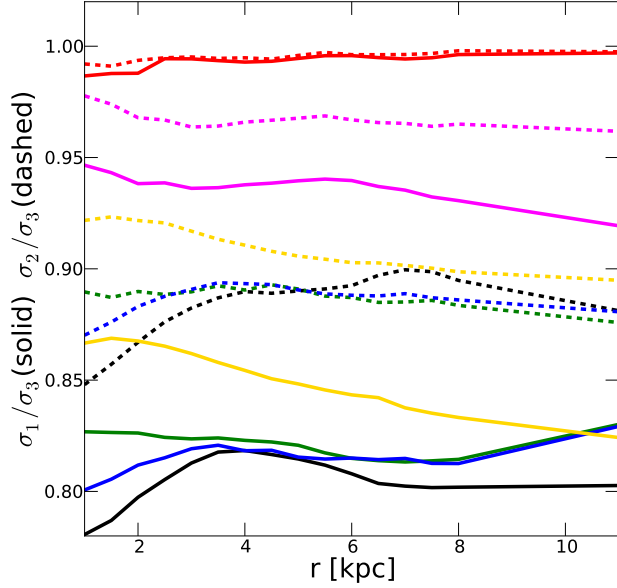


**Figure 6.** Ratios of the components of the diagonal velocity dispersion tensor  $\sigma_1 < \sigma_2 < \sigma_3$  measured in different radial shells for the different DM models. We show the smallest-to-largest ( $\sigma_1/\sigma_3$ ) and intermediate-to-largest ( $\sigma_2/\sigma_3$ ) ratios. Colours are as in Fig. 1. The velocity dispersion tensor in the SIDM10 case is essentially isotropic in the inner halo with  $\sigma_1/\sigma_3 \sim \sigma_2/\sigma_3 \sim 1$ , while the other constant cross section cases (SIDM1, SIDM0.1) show a gradual increase in the degree of anisotropy with decreasing cross section. The vdSIDM models have ratios very close to the CDM case and are clearly anisotropic and very distinct from the models with a constant cross section.

et al. 2010). Also the DM phase-space structure will be affected by baryons, which will also alter the detection signal. The impact of baryonic processes would likely be quite different in SIDM than in CDM (especially for subhaloes) and goes beyond the scope of the present study, since our goal is to compare the differences with CDM driven purely by DM self-scattering.

#### 4 VELOCITY STRUCTURE OF THE INNER HALO

The local velocity structure is important for direct detection experiments since the interaction rate is proportional to the  $1/v$ -weighted integral over the local velocity distribution (see below). To explore the velocity structure we measure the distribution of the local velocity modulus at different halocentric distances (2 kpc, 5 kpc, 8 kpc). At each distance we construct histograms in  $v$  for all particles within spheres of 1 kpc radius sampled at the three different radii for 1000 randomly selected observers. Fig. 4 shows the resulting distributions for the different halocentric distances. We show the median velocity distribution (thick lines) and 10 – 90% quantiles (shaded regions) to indicate the scatter at different random positions at a given halocentric distance. The left three panels of Fig. 4 show the actual distributions, whereas the right panels show the median of the ratio of the distribution for the SIDM models to the distribution of the CDM case over the sample of all observers. Clearly, the distribution for the SIDM10 case (with the largest constant cross section) is significantly smoother due to the large number of isotropic scatterings through the halo history. The bumps and wiggles that are present in the CDM case, and that re-

fect the assembly history of the halo (Vogelsberger et al. 2009), are largely preserved for vdSIDMa, vdSIDMb and SIDM0.1, but are essentially washed out for SIDM10 and significantly reduced for SIDM1. Notice that despite the relatively low constant cross section in SIDM0.1, it still produces a distinct velocity distribution from that of the CDM case. For all models the largest difference with the collisionless case occurs for the innermost radial distance where the density is higher leading to the highest number of scattering events. For vdSIDMa, vdSIDMb and SIDM0.1, the differences become smaller with increasing halocentric distance since scattering events become less likely. In the former two cases the scattering rate decreases more rapidly with radius because of the steep velocity dependence of the cross section. We note that also the scatter of the distributions agrees very well between all models at large distances, which indicates a very similar velocity structure in the halo at these halocentric distances. Only the models SIDM and SIDM1 have non-negligible deviations for  $r \sim 8$  kpc since they still produce a relatively large scattering rate even at these distances. The dashed black line in the left panels of Fig. 4 shows a Maxwell-Boltzmann distribution with  $\sigma_{1D} = 151.6 \text{ km s}^{-1}$ , which fits the SIDM results well, demonstrating that self-interactions lead in that case to a significant thermalisation of the inner halo. The distribution of SIDM1 (with a ten times smaller cross section) cannot be fitted exactly by a Maxwell-Boltzmann distribution, but is still quite close, whereas all other models clearly have very different distributions.

When there are several collisions per particle, the velocity distribution tends to be thermalised (i.e., it becomes Maxwellian). This clearly happens at small radii for the cases of large constant cross section, as we mentioned in the previous section. In this process, particles from the low and high velocity tails are transferred towards intermediate velocities. When the number of collisions is low, however, the distribution is not fully thermalised and it is modified only slightly in a more discrete way. At the high-end of the velocity distribution, the cases with a constant cross section preferentially scatter these high velocity particles with those with lower velocities (since their number density is higher). Since scatter happens elastically, the high velocity particles end up with lower velocities and hence, the particle number density in the velocity tail is lower than in the CDM case. For the vdSIDM cases on the other hand, there is a selection effect in the scattering process for particles that are moving roughly in the same direction and speed (in order to have low relative velocities). Thus, particles in the high-end velocity tail collide with others in the tail as well and this leaves the velocity distribution essentially unchanged.

CDM haloes have a velocity structure that is anisotropic (e.g. Navarro et al. 2010). Since we are only considering isotropic scattering, i.e., the velocities are redistributed on the unit sphere after a scatter event, a large number of scattering events should lead to a velocity structure that is less anisotropic than in the CDM case. The difference is more important near the center where the scattering rate is higher. To test this we show in Fig. 5 the distribution of the largest and smallest principal components of the velocity ellipsoid: specifically, for each of the observer’s 1 kpc spheres, we calculate the local velocity ellipsoid and project the velocity along the principal axes. As in Fig. 4, the left panels show the distribution at different halocentric distances, whereas the right panels show the deviations of each of the SIDM cases relative to the CDM case. Most strikingly, the large number of scatter events in the SIDM10 case produces an almost fully isotropic distribution at all radii within  $\sim 8$  kpc of the main halo (which is roughly the size of the core induced by self-scattering, see VZL). The compo-



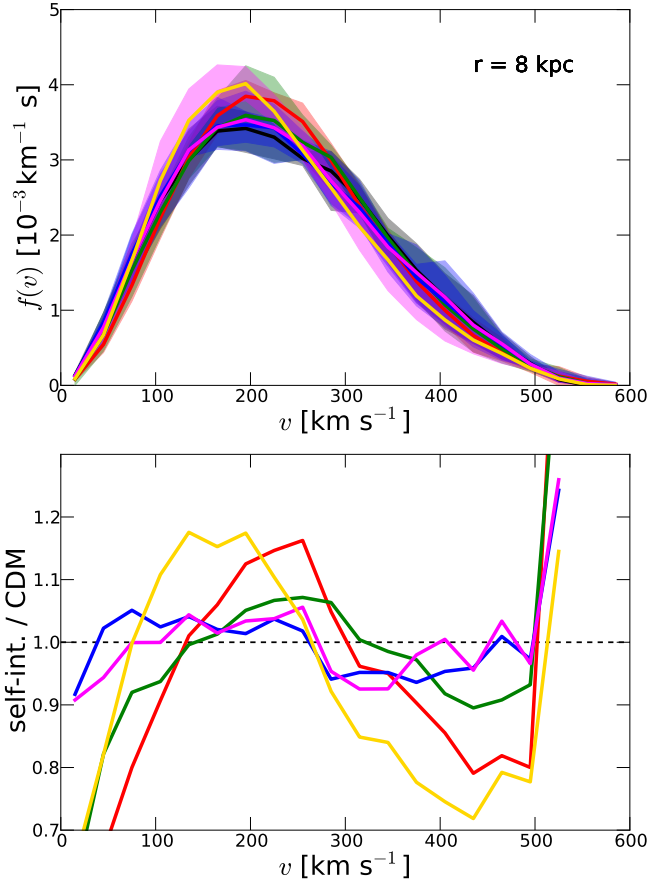


**Figure 7.** Velocity distribution as in Fig. 4, but for a sample of different MW-size haloes (Aq-A-4 to Aq-F-4). Top panel: Distribution of the velocity modulus measured at 8 kpc from the halo centre. For each halo and halo, we first measure the velocity distribution in 1000 randomly selected spheres of 1 kpc radius at the indicated distances, and then calculate the median over all observers for each model and halo. We then take the mean of these median distributions over all haloes to derive the average distribution for each model (solid lines). The shaded regions show the range of distributions that is spanned by the individual medians of all haloes for a given model, i.e., this shows the halo-to-halo scatter of the medians. Bottom panel: Ratio of the medians of the different models to the CDM case. The two panels demonstrate that the trends found for the halo sample (Aq-A-4 to Aq-F-4) are essentially the same as those found for the single halo in Fig. 4. Thus, these findings are robust with respect to cosmic variance and should hold for generic haloes in the mass range of our own MW halo.

nents of the velocity ellipsoid are Gaussian with a nearly identical variance which leads to a nearly Maxwellian distribution for the modulus of the velocity vector as we have shown in Fig. 4. The ratios of the dispersions of the principal components  $\sigma_1 < \sigma_2 < \sigma_3$  for each case are shown in Fig. 6 as a function of radius. This plot shows more clearly the degree of anisotropy in the velocity distributions. SIDM10 is essentially isotropic in the inner halo with  $\sigma_1/\sigma_3$  and  $\sigma_2/\sigma_3$  being close to unity, while the other constant cross section models (SIDM1, SIDM0.1) show a gradual increase on the anisotropy; particularly towards large radii where the scattering rate is lower. On the other hand, the vdSIDM models are just slightly more isotropic than CDM.

So far we have focused our analysis only on one specific halo. We will now explore how the velocity results presented above change if we consider different haloes. Fig. 7 shows for each DM

model the distribution of the velocity modulus for different haloes measured at 8 kpc halocentric distance. For each halo the measurement is done exactly the same way as described above for Aq-A. The thick lines show the mean over all haloes (Aq-A-4 to Aq-F-4) for each model. The shaded region encloses the distribution of all haloes for each model. The trends found for this halo sample are essentially the same as those found for the single halo in Fig. 4. I.e., these trends are robust with respect to cosmic variance and should hold for generic haloes in the mass range of our own Milky Way halo. We have also checked that this is true for different halocentric distances. Based on this, we conclude that the results found for Aq-A-3 should hold for generic MW-sized haloes.

## 5 DIRECT DETECTION SIGNAL

The DM phase-space structure directly affects the detection rate for experiments that are looking for DM particles signals. As demonstrated above, significant DM self-scattering leads to a different DM velocity distribution and we examine now the expected impact on the recoil rates.

The DM-nucleon scattering event rate is given by (e.g. Jungman et al. 1996):

$$R(E, t) = \mathcal{R} \rho_0 T(E, t) = \mathcal{R} \rho_0 T(v_{\min}(E), t), \quad (1)$$

where  $\mathcal{R}$  encapsulates the particle physics parameters (mass and cross section of the DM particle; form factor and mass of the target nucleus),  $\rho_0$  is the local dark matter density, and the local velocity distribution enters in an integrated form as:

$$T(v_{\min}(E), t) = \int_{v_{\min}(E)}^{\infty} \frac{f_v(t)}{v} dv, \quad v_{\min}(E) = \left( \frac{E (m_\chi + m_N)^2}{2m_\chi^2 m_N} \right)^{1/2}, \quad (2)$$

where  $f_v$  is the DM speed distribution in the rest frame of the detector integrated over the angular distribution;  $v_{\min}(E)$  is the minimum DM particle speed (detector-dependent) that can cause a recoil of energy  $E$ . This threshold velocity depends on the DM particle mass  $m_\chi$  and nuclear mass of the target  $m_N$ . Since we are primarily interested in the impact of different velocity distributions, we focus in the following on  $T(v_{\min}, t)$  rather than  $R(E, t)$  which is more sensitive to the details of the detector and particle physics.

The velocity distribution function depends on time because of the motion of the Earth with respect to the galactic halo. This produces an annual modulation in the recoil rate. We parametrise the motion of the Earth following (Kerr & Lynden-Bell 1986; Lewin & Smith 1996; Dehnen & Binney 1998), and refer the reader to Vogelsberger et al. (2009) for the detailed parametrisation. For definitiveness, we fix the value of  $t$  to two days during the course of a year when calculating the recoil rate spectrum  $T(v_{\min}, t)$ . Specifically, these are day 153 (June 2nd) and 336 (December 2nd) of 2013 (left panels of Fig. 8). These days are close to the extrema of the modulation signal. The right panels of Fig. 8 show the ratio of the  $T(v_{\min}, t)$  recoil rates relative to the vanilla CDM model for the different SIDM models. We note that these rates and the ratios were calculated at 8 kpc halocentric distance and, as above, for 1000 randomly selected spheres of 1 kpc radius. Black dashed lines in each panel show the expected detector signal for the Maxwell-Boltzmann ( $\sigma_{1D} = 151.6 \text{ km s}^{-1}$ ) distribution shown in Fig. 4, which fits the velocity distribution of SIDM10 best and is quite similar to the standard halo model.

The relative variation between the different models does not

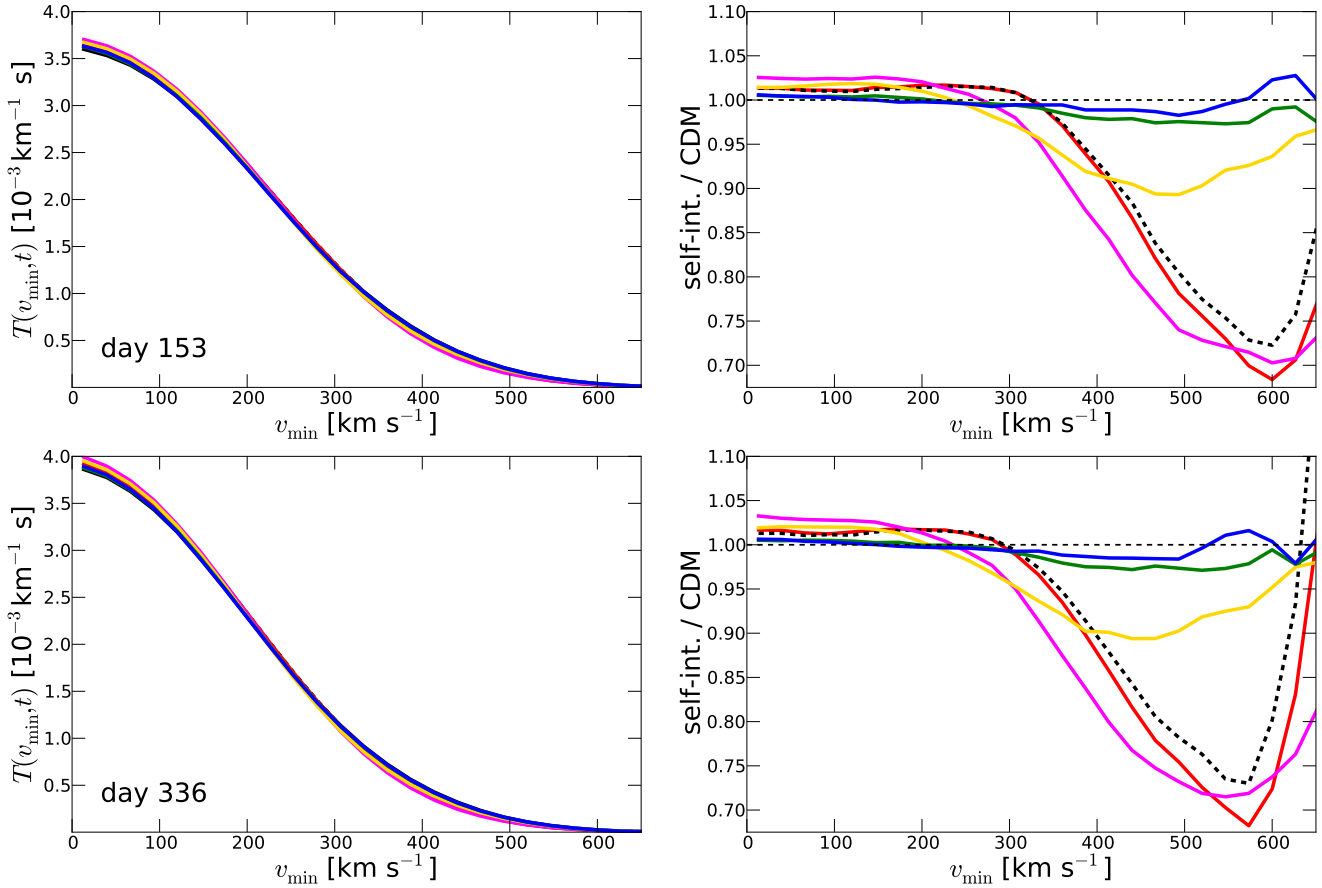


**Figure 8.** Left panels: Detector recoil rates ( $T(v_{\min}, t)$ ) for the different DM models. We show the median signal for 1000 randomly selected observers at the solar circle (8 kpc halocentric distance), where the detector signal is sampled within spheres of 1 kpc radius. The selected two days correspond to June 2nd (day 153) and December 2nd (day 336) of 2013. Right panels: Median of ratios of the SIDM models relative to the local CDM case for all observers. Colours are as in Fig. 1. The low energy distribution shows only minor changes with respect to the CDM case for all models ( $\lesssim 5\%$ ) with the vdSIDM models showing essentially no deviation (percent level) from the CDM case. Above  $v_{\min} \sim 250 \text{ km s}^{-1}$  the constant cross section models start to deviate significantly from CDM showing strongly reduced recoil rates. For SIDM0.1, the ratio is smallest around  $v_{\min} \sim 450 \text{ km s}^{-1}$ , where the SIDM rate is about 10% smaller than the CDM prediction. SIDM10 and SIDM1 both have their largest deviation from the CDM case at about  $v_{\min} \sim 600 \text{ km s}^{-1}$ . Although these two models differ by a factor of 10 in their cross section, they both have a recoil rate which is approximately 30% smaller than that of CDM around that velocity. Black dashed lines in each panel show the expected detector signal for the Maxwell-Boltzmann distribution ( $\sigma_{\text{ID}} = 151.6 \text{ km s}^{-1}$ ) shown in Fig. 4, which fits the velocity distribution of SIDM10 best and is quite similar to the standard halo model.

seem to depend strongly on the day of the year. For all models, the low energy distribution shows only very minor changes with respect to the CDM case. These differences are at maximum 5% for the most extreme constant cross section models (SIDM10, SIDM1), while there is essentially no deviation (percent level) for the vdSIDM models. Above  $v_{\min} \sim 250 \text{ km s}^{-1}$  all constant cross section models start to deviate significantly from CDM showing lower recoil rates. For SIDM0.1 the ratio is smallest around  $v_{\min} \sim 450 \text{ km s}^{-1}$ , where the SIDM rate is about 10% smaller than the CDM prediction. SIDM10 and SIDM1, which have 100 and 10 times larger constant cross sections than SIDM0.1, both have their largest deviation from the CDM case at about  $v_{\min} \sim 600 \text{ km s}^{-1}$ . Although these two models differ by a factor of 10 in their cross section, they both have a recoil rate which is approximately 30% smaller than that of CDM around that velocity. Interestingly, self-interaction only leads to a reduction of the recoil rates with respect to the CDM case. I.e., except for the very small increase towards lower recoil energies, we do not find a regime where the recoil rate is increased significantly.

To make connection with experimental efforts, Table 3 lists

Experiment	$E_{\text{thres}}$ [keV]	$v_{\min, \text{thres}}^{m_\chi=10 \text{ GeV}}$ [km s $^{-1}$ ]
CDMS-Si	7	398
CRESST-O-band	15	527
COGENT-Ge	1.9	282
DAMA-Na	6.7	371
Xenon	2	361

**Table 3.** Typical threshold energies and corresponding  $v_{\min}$  values for current experiments with different detector materials (Si, O, Ge, Na, Xe). Taken from Fox et al. (2011) (see their Fig. 1). For such a particle (and heavier ones), most of the current experiments have  $v_{\min}$  thresholds below the value where we expect to see a significant difference in the recoil rates due to self-scattering (see Fig. 8). This means that most experiments should be sensitive to the effects of self-interacting DM.

the threshold recoil energies ( $E_{\text{thres}}$ ) for a few experiments and the corresponding  $v_{\min, \text{thres}}$  values for a  $m_\chi = 10 \text{ GeV}$  DM particle. For such a particle (and heavier ones), most of current experiments have  $v_{\min}$  thresholds below the value where we expect to see a

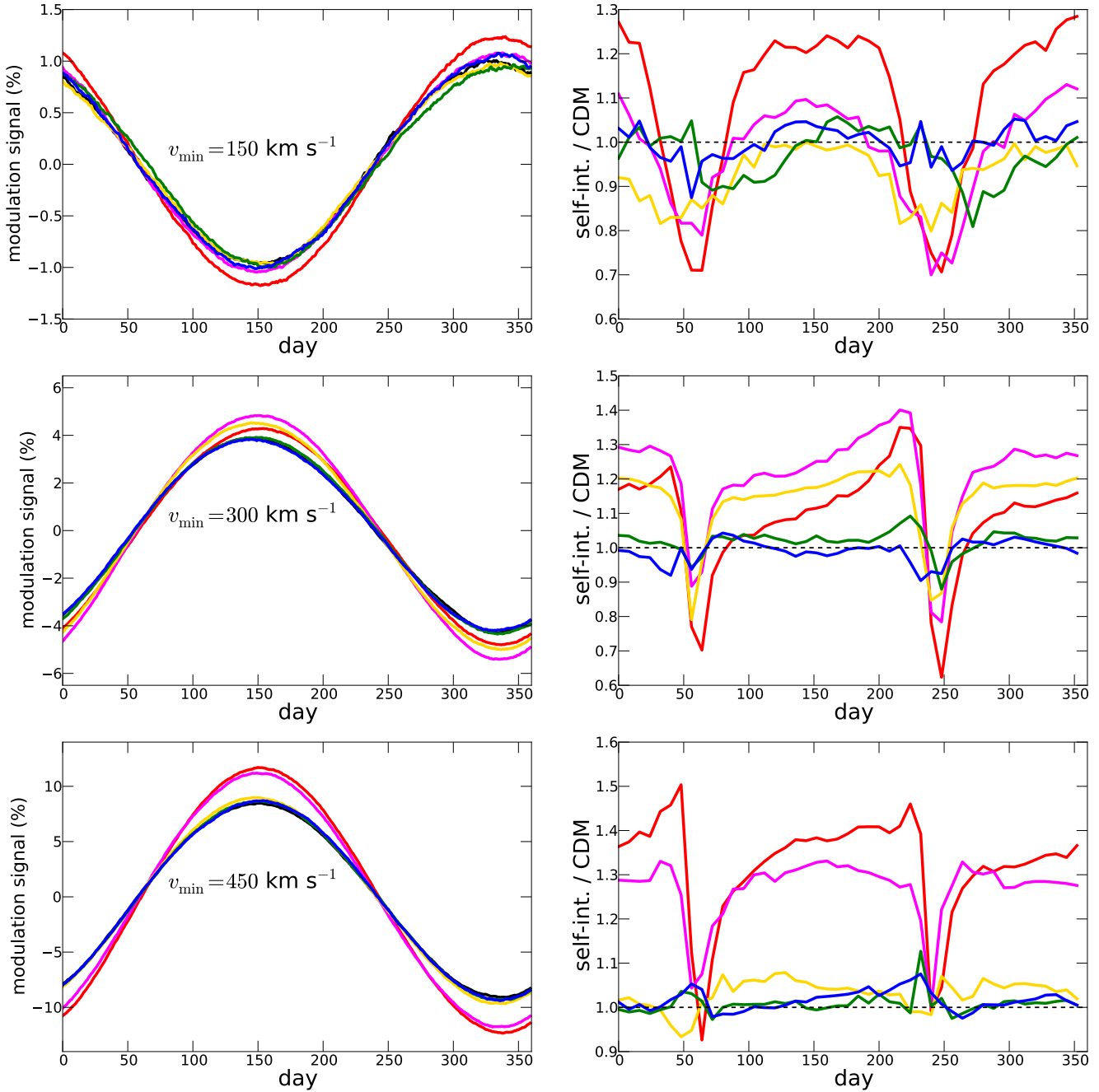


**Figure 9.** Left panels: Median annual modulation signal of 1000 randomly selected spheres (1 kpc radius) at 8 kpc halocentric distance for different recoil energies as indicated by the corresponding  $v_{\min}$  velocities. Colours are as in Fig. 1. Right panel: Median of the ratio of the SIDM models over the CDM prediction. Depending on the DM model, the modulation amplitude can differ from the CDM prediction by up to 40%. Furthermore, self-interaction induces a change in the day of the peak of the modulation such that this day varies by about two weeks for the different models.

significant difference in the recoil rates due to self-scattering (see Fig. 8). This implies that these experiments should actually be sensitive to the effects of self-scattering and, in principle, they should be able to distinguish different constant and velocity-dependent models. However, elastic scattering rates are dominated by the lowest recoil energies, thus, experiments with  $v_{\min} \lesssim 300 \text{ km s}^{-1}$ , which is where SIDM effects start to be important, are mostly dominated by events for which the scattering rate is indistinguishable from CDM. Because of this, experiments with a larger threshold energy, in the range where SIDM effects are maximised, are bet-

ter suited to detect the imprints of self-interacting DM. Of the experiments listed in Table 3 CDMS-Si and CRESST (oxygen band) operate in this regime (this is of course mass dependent, DM particles lighter than  $m_{\chi} = 10 \text{ GeV}$  would have higher thresholds, and vice versa). It is important to mention, however, that distinguishing different dark matter models using a detector signal might be challenging in current experiments due to the associated errors in the recoil rates. For instance for CoGENT and CRESST, the relative error in the number of events observed by the detectors near threshold is  $\sim 10 - 20\%$  (see Figs. 3 and 4 of Hooper et al. 2010),

which is of the order of the differences we expect between allowed SIDM models and CDM.

We note that the interpretation of most direct detection results assume a simple standard halo model with a Maxwell-Boltzmann distribution to infer, for example, limits on particle cross-sections and masses. Typically the one-dimensional velocity dispersion is then either assumed to be  $\sigma_{1D} = 156 \text{ km s}^{-1}$  or taken directly from a fit to CDM simulations. We find that the most extreme SIDM model (SIDM10) establishes a Maxwell-Boltzmann distribution quite close to the one assumed in the standard halo model: we found a best fit with  $\sigma_{1D} = 151.6 \text{ km s}^{-1}$ , just slightly lower than the standard assumption. However, the SIDM cases of interest, those not ruled out by other observations, show significant departures from the standard halo, which implies that the simplified assumptions about the halo velocity structure are not valid for self-interacting DM.

The present DAMA/LIBRA experiment and the former DAMA/NaI one have reported an annual modulation signal from results corresponding to a total exposure of  $1.17 \text{ ton} \times \text{yr}$  over 13 annual cycles with a confidence level of  $8.9\sigma$  (Bernabei et al. 2012). Such a signal is expected from DM due to the motion of the Earth through the galactic halo. Since self-scattering changes the DM velocity distribution and, hence, the detector signal, it is expected that the annual modulation signal will also be sensitive to self-interactions of DM particles. In Fig. 9, we show the annual modulation signal of the different DM models for three different recoil energies given by three different minimum velocities,  $v_{\min} = 150 \text{ km s}^{-1}$  (top),  $300 \text{ km s}^{-1}$  (middle),  $450 \text{ km s}^{-1}$  (bottom). The left panels show the actual modulation signal, whereas the right panels show the median ratios of the non-CDM models to the CDM case. To avoid too much noise in this ratio, we show it only for every 4th day, whereas the actual modulation signal is sampled for each day.

The qualitative difference between the  $v_{\min} = 150 \text{ km s}^{-1}$  modulation signal and the other two values of  $v_{\min}$  is due to the phase reversal effect (e.g. Primack et al. 1988; Lewis & Freese 2004), which is consistently observed for all DM models. This phase reversal occurs below a critical recoil energy, which is a function of the mass of the DM particle, as well as the nuclear mass of the target. We find that it also depends on how collisionless is DM. For definiteness, we take the time of reversal as the first time when the day of maximum amplitude is not close to day  $\sim 300$ , but rather jumps to about  $> 100$  days earlier. With this definition we find for the time of phase reversal (CDM, SIDM10, SIDM1, SIDM0.1, vdSIDMa, vdSIDMb): 177, 185, 177, 172, 176, 180, i.e., SIDM0.1 changes first around day 172 and SIDM10 changes phase about 13 days later. The time of phase reversal of the the different DM models therefore spans about two weeks, which provides a good probe to distinguish between different (non-) self-interacting DM candidates.

The modulation signal clearly depends on the particular DM model. As expected, based on the results presented in the previous Sections, SIDM10 and SIDM1 lead to the largest deviations from the CDM modulation signal. For all recoil energies, these modulation signals deviate by about 30% from the CDM case. (we note that the best fit amplitude in the modulation signal reported by DAMA/NaI and DAMA/LIBRA experiments has a relative error of  $\sim 10\%$ , Bernabei et al. 2012). For  $v_{\min} = 300 \text{ km s}^{-1}$ , not only does the amplitude changes, but also a clear shift of the peak is visible for the constant cross section models. This shift is largest for SIDM10, but still clearly present for SIDM1 and to some degree also for SIDM0.1. The days with the indicated ampli-

tudes for CDM, SIDM10, SIDM1, SIDM0.1, vdSIDMa, vdSIDMb are: 141 (3.8%), 156 (4.3%), 142 (4.8%), 151 (4.6%), 146 (3.9%), 137 (3.8%). The vdSIDM models lead only to variations of the order of 10% in the modulation amplitude. For the recoil energy corresponding to  $v_{\min} = 450 \text{ km s}^{-1}$ , the vdSIDM models and SIDM0.1 lead only to very small differences ( $< 10\%$ ) from the CDM case. In most of the SIDM models, the modulation amplitude is increased compared to the CDM case for most of the days during the year, especially for  $v_{\min} = 300 \text{ km s}^{-1}$ , where all models show a rapid decrease in the otherwise higher modulation signal. The days when this happens correspond to the days in the left panels where the different modulation signals cross the CDM signal.

## 6 SUMMARY AND CONCLUSIONS

Definitive proof for the existence of DM as a new particle beyond the Standard Model of particle physics is expected to come from laboratories on Earth that are looking for the collision of dark matter with nuclei in target detectors. The hypothetical interaction rate depends on the intrinsic properties of the dark matter (DM) particle and on the phase-space DM distribution at the scale of the detector. Thus, interpreting a positive signal or deriving a constraint on the DM properties based on a null result, can only be done reliably through a detailed knowledge of its local phase space distribution. The most powerful approach to accomplish this is through the use of numerical simulations that follow the formation and evolution of DM structures through cosmic time. These simulations have already been used to report significant differences over the traditional assumptions of a smooth density distribution and a Maxwellian velocity distribution (Vogelsberger et al. 2009; Kuhlen et al. 2010). To date, all predictions for direct detection experiments from numerical simulations have been obtained within the context of the Cold Dark Matter (CDM) paradigm. It is possible, however, that DM has a non-negligible self-scattering cross section, large enough to have a significant impact at galactic scales and yet, sufficiently small to satisfy current astrophysical constraints (Vogelsberger et al. 2012; Rocha et al. 2012; Peter et al. 2012). The interest in self-interacting DM (SIDM) models has been renewed recently, since they are able to successfully reduce the central densities of dark matter (sub)haloes and create dark matter cores that are seemingly consistent with observations of dwarf galaxies (Boylan-Kolchin et al. 2011; Vogelsberger et al. 2012; Rocha et al. 2012).

In this paper we present the first study on the impact of DM self-scattering on the velocity distribution of dark matter haloes and on the anticipated direct detection signals. We imagine a particle physics scenario where dark matter strongly interacts with itself but interacts with nuclei at the level probed by current DM detectors (a possible scenario would be along the lines of the models proposed in Fornengo et al. (2011) and Hooper et al. (2012), see also Cyr-Racine & Sigurdson (2012) for a different plausible model). Although it is expected that DM collisions will tend to modify the collisionless velocity distribution towards a Maxwellian one, we quantify this in detail by re-simulating the MW-size Aquarius haloes (Springel et al. 2008) within the context of SIDM using the algorithm described in Vogelsberger et al. (2012) (VZL). We study five different SIDM models, three with a constant cross section: SIDM10 ( $\sigma_T/m_\chi = 10 \text{ cm}^2 \text{ g}^{-1}$ , ruled-out by observations), SIDM1 ( $\sigma_T/m_\chi = 1 \text{ cm}^2 \text{ g}^{-1}$ , likely ruled out) and SIDM0.1 ( $\sigma_T/m_\chi = 0.1 \text{ cm}^2 \text{ g}^{-1}$ , consistent with observations), and two with a velocity-dependent cross section (allowed by current observations and studied in VZL within the model of Loeb & Weiner

(2011)). It was demonstrated in VZL that the latter two models can also alleviate the tension between the MW's dSphs and theoretical predictions.

We find that all SIDM models show a significant departure from the velocity distribution of the CDM model in the center of the MW halo (within  $\sim 2$  kpc), while at the solar circle the scattering effect is less significant (see Fig. 4). Only the cases with constant cross section still show a significant difference relative to the CDM prediction. Particularly, those with the largest cross section ( $\sigma_T/m_\chi > 1 \text{ cm}^2 \text{ g}^{-1}$ ) result in a velocity distribution that is essentially Maxwellian at the solar circle. In these cases, the distribution within  $\sim 10$  kpc can be described very well by a Maxwell-Boltzmann distribution function with a one-dimensional velocity dispersion of  $\sigma_{1D} \sim 152 \text{ km s}^{-1}$ , which is quite close to the value of  $156 \text{ km s}^{-1}$  assumed in the standard halo model. On the other hand, although the case with a self-scattering cross section of  $\sigma_T/m_\chi = 0.1 \text{ cm}^2 \text{ g}^{-1}$  also shows distinct deviations from the CDM distribution ( $\lesssim 20\%$ ), its distribution is clearly non-Maxwellian. The velocity-dependent SIDM cases show even smaller departures from CDM ( $< 5\%$ ). We note that the latter three models (vdSIDMa, vdSIDMb, SIDM0.1) are all consistent with current observational constraints. In addition to thermalising the velocity distribution, DM scatterings also isotropized the orbits, which we clearly observe by looking at the principal components of the velocity dispersion tensor (see Figs. 5 and 6). However, only the constant cross section models show considerable departures from an anisotropic distributions. Models with a velocity dependent cross section are very close to CDM in the inner halo.

The differences in the velocity distribution impact the predicted recoil rates in direct detection experiments. This depends on the recoil energy, corresponding to a minimum velocity  $v_{\min}$  of the DM particles necessary to impart a measurable recoil in a given detector. We find that the recoil rates begin to deviate significantly from the CDM predictions for  $v_{\min} > 250 \text{ km s}^{-1}$ , being lower by as much as 30% for the largest constant cross section cases, and only at the percent level for the vdSIDM cases (see Fig. 8). These changes occur in a recoil energy range currently accessible by essentially all direct detection experiments. Models that are fully consistent with current observational constraints can lead to a deviation of about 10%.

We also find differences between the SIDM models and CDM in the amplitude and peak days of the annual modulation signal (see Fig. 9). The former is larger by as much as 40% (25% for allowed models) while the latter is shifted by two weeks at the most. Interestingly, we find a significant shift in the day when the well-known phase reversal effect of the modulation signal (e.g. Primack et al. 1988; Lewis & Freese 2004) occurs. The time of phase reversal of the the different DM models spans about two weeks, which therefore provides a sensitive probe to distinguish between different (non-) self-interacting DM candidates. Even the cases where the scattering cross section is velocity-dependent show a distinct phase reversal shift by a couple of days.

We conclude that direct detection experiments should in principle be sensitive to currently allowed SIDM models. In general models with velocity dependent cross sections peaking at the typical velocities of dwarf galaxies lead only to minor changes in the detection signals, whereas allowed constant cross section models lead to significant changes.

## ACKNOWLEDGEMENTS

We thank Volker Springel for giving us access to GADGET-3, Philippe Di Stefano and Naoki Yoshida for initial discussions that inspired this work, Adrian Jenkins for generating the initial conditions of Aq-F-4, Adrienne Erickcek, Lars Hernquist, Michael Kuhlen, Avi Loeb, Josef Pradler, Kris Sigurdson, Paul Torrey and Simon White for useful suggestions. JZ is supported by the University of Waterloo and the Perimeter Institute for Theoretical Physics. Research at Perimeter Institute is supported by the Government of Canada through Industry Canada and by the Province of Ontario through the Ministry of Research & Innovation. JZ acknowledges financial support by a CITA National Fellowship. MV acknowledges support from NASA through Hubble Fellowship grant HST-HF-51317.01.

## REFERENCES

- Abel T., Hahn O., Kaehler R., 2011, ArXiv e-prints  
 Arkani-Hamed N., Finkbeiner D. P., Slatyer T. R., Weiner N., 2009, Phys. Rev. D, 79, 015014  
 Bernabei R., Belli P., Di Marco A., Montecchia F., Cappella F., d'Angelo A., Incicchitti A., Prosperi D., Cerulli R., Dai C. J., He H. L., Ma X. H., Sheng X. D., Wang R. G., Ye Z. P., 2012, Nuclear Instruments and Methods in Physics Research A, 692, 120  
 Bertone G., Hooper D., Silk J., 2005, Phys. Rep., 405, 279  
 Bode P., Ostriker J. P., Turok N., 2001, ApJ, 556, 93  
 Boyarsky A., Ruchayskiy O., Iakubovskiy D., 2009, Journal of Cosmology and Astroparticle Physics, 3, 5  
 Boylan-Kolchin M., Bullock J. S., Kaplinghat M., 2011, MNRAS, 415, L40  
 Buckley M. R., Fox P. J., 2010, Phys. Rev. D, 81, 083522  
 Colín P., Avila-Reese V., Valenzuela O., 2000, ApJ, 542, 622  
 Cyr-Racine F.-Y., Sigurdson K., 2012, ArXiv e-prints  
 Dehnen W., Binney J. J., 1998, MNRAS, 298, 387  
 Diemand J., Kuhlen M., Madau P., Zemp M., Moore B., Potter D., Stadel J., 2008, Nature, 454, 735  
 D'Onghia E., Springel V., Hernquist L., Keres D., 2010, ApJ, 709, 1138  
 Erickcek A. L., Steinhardt P. J., McCammon D., McGuire P. C., 2007, Phys. Rev. D, 76, 042007  
 Fornengo N., Panci P., Regis M., 2011, Phys. Rev. D, 84, 115002  
 Fox P. J., Liu J., Weiner N., 2011, Phys. Rev. D, 83, 103514  
 Hooper D., Collar J. I., Hall J., McKinsey D., Kelso C. M., 2010, Phys. Rev. D, 82, 123509  
 Hooper D., Weiner N., Xue W., 2012, Phys. Rev. D, 86, 056009  
 Jungman G., Kamionkowski M., Griest K., 1996, Phys. Rep., 267, 195  
 Kerr F. J., Lynden-Bell D., 1986, MNRAS, 221, 1023  
 Kuhlen M., Lisanti M., Spergel D. N., 2012, Phys. Rev. D, 86, 063505  
 Kuhlen M., Vogelsberger M., Angulo R., 2012, ArXiv e-prints  
 Kuhlen M., Weiner N., Diemand J., Madau P., Moore B., Potter D., Stadel J., Zemp M., 2010, J. Cosmol. Astropart. Phys., 2, 30  
 Lewin J. D., Smith P. F., 1996, Astroparticle Physics, 6, 87  
 Lewis M. J., Freese K., 2004, Phys. Rev. D, 70, 043501  
 Loeb A., Weiner N., 2011, Physical Review Letters, 106, 171302  
 Navarro J. F., Eke V. R., Frenk C. S., 1996, MNRAS, 283, L72  
 Navarro J. F., Ludlow A., Springel V., Wang J., Vogelsberger M., White S. D. M., Jenkins A., Frenk C. S., Helmi A., 2010, MNRAS, 402, 21

- Neyrinck M. C., Shandarin S. F., 2012, ArXiv e-prints
- Peter A. H. G., Rocha M., Bullock J. S., Kaplinghat M., 2012, ArXiv e-prints
- Pontzen A., Governato F., 2012, MNRAS, 421, 3464
- Primack J. R., Seckel D., Sadoulet B., 1988, Annual Review of Nuclear and Particle Science, 38, 751
- Rocha M., Peter A. H. G., Bullock J. S., Kaplinghat M., Garrison-Kimmel S., Onorbe J., Moustakas L. A., 2012, ArXiv e-prints
- Spergel D. N., Steinhardt P. J., 2000, Physical Review Letters, 84, 3760
- Springel V., 2005, MNRAS, 364, 1105
- Springel V., Wang J., Vogelsberger M., Ludlow A., Jenkins A., Helmi A., Navarro J. F., Frenk C. S., White S. D. M., 2008, MNRAS, 391, 1685
- Springel V., White S. D. M., Jenkins A., Frenk C. S., Yoshida N., Gao L., Navarro J., Thacker R., Croton D., Helly J., Peacock J. A., Cole S., Thomas P., Couchman H., Evrard A., Colberg J., Pearce F., 2005, Nature, 435, 629
- Stadel J., Potter D., Moore B., Diemand J., Madau P., Zemp M., Kuhlen M., Quilis V., 2009, MNRAS, 398, L21
- van den Aarssen L. G., Bringmann T., Pfrommer C., 2012, ArXiv e-prints
- Vogelsberger M., Helmi A., Springel V., White S. D. M., Wang J., Frenk C. S., Jenkins A., Ludlow A., Navarro J. F., 2009, MNRAS, 395, 797
- Vogelsberger M., White S. D. M., 2011, MNRAS, 413, 1419
- Vogelsberger M., White S. D. M., Helmi A., Springel V., 2008, MNRAS, 385, 236
- Vogelsberger M., White S. D. M., Mohayaee R., Springel V., 2009, MNRAS, 400, 2174
- Vogelsberger M., Zavala J., Loeb A., 2012, MNRAS, 423, 3740
- Weinberg M. D., Katz N., 2002, ApJ, 580, 627
- White S. D. M., Vogelsberger M., 2009, MNRAS, 392, 281
- Wu H.-Y., Hahn O., Wechsler R. H., Mao Y.-Y., Behroozi P. S., 2012, ArXiv e-prints
- Yoshida N., Springel V., White S. D. M., Tormen G., 2000, ApJ, 544, L87
- Zavala J., Jing Y. P., Faltenbacher A., Yepes G., Hoffman Y., Gottlöber S., Catinella B., 2009, ApJ, 700, 1779
- Zavala J., Vogelsberger M., Walker M. G., 2012, arXiv:1211.6426